land

MDPI

Article

Detectability of the Critically Endangered *Araucaria angustifolia* Tree Using Worldview-2 Images, Google Earth Engine and UAV-LiDAR

Felipe Saad [1,*], Sumalika Biswas [2], Qiongyu Huang [2], Ana Paula Dalla Corte [3], Márcio Coraiola [4], Sarah Macey [2], Marcos Bergmann Carlucci [5] and Peter Leimgruber [2]

1 Programa de Pós-Graduação em Ecologia e Conservação, Universidade Federal do Paraná, Curitiba 81531-980, Brazil
2 Smithsonian Conservation Biology Institute, Front Royal, VA 22630, USA; sumalika.biswas@gmail.com (S.B.); HuangQ@si.edu (Q.H.); maceys@vt.edu (S.M.); LeimgruberP@si.edu (P.L.)
3 Centro de Excelência em Pesquisas sobre Fixação Carbono na Biomassa—BIOFIX Lab, Universidade Federal do Paraná, Curitiba 81530-00, Brazil; anacorte@ufpr.br
4 Engenharia Florestal, Pontifícia Universidade Católica do Paraná—PUCPR, Curitiba 80215-901, Brazil; marciocoraiola@gmail.com
5 Laboratório de Ecologia Funcional de Comunidades (LABEF), Departamento de Botânica, Universidade Federal do Paraná, Curitiba 81531-980, Brazil; carlucci@ufpr.br
* Correspondence: fsaad1@umbc.edu

Abstract: The Brazilian Atlantic Forest is a global biodiversity hotspot and has been extensively mapped using satellite remote sensing. However, past mapping focused on overall forest cover without consideration of keystone plant resources such as *Araucaria angustifolia*. *A. angustifolia* is a critically endangered coniferous tree that is essential for supporting overall biodiversity in the Atlantic Forest. *A. angustifolia's* distribution has declined dramatically because of overexploitation and land-use changes. Accurate detection and rapid assessments of the distribution and abundance of this species are urgently needed. We compared two approaches for mapping *Araucaria angustifolia* across two scales (stand vs. individual tree) at three study sites in Brazil. The first approach used Worldview-2 images and Random Forest in Google Earth Engine to detect *A. angustifolia* at the stand level, with an accuracy of >90% across all three study sites. The second approach relied on object identification using UAV-LiDAR and successfully mapped individual trees (producer's/user's accuracy = 94%/64%) at one study site. Both approaches can be employed in tandem to map remaining stands and to determine the exact location of *A. angustifolia* trees. Each approach has its own strengths and weaknesses, and we discuss their adoptability by managers to inform conservation of *A. angustifolia*.

Keywords: Atlantic Forest; *Araucaria angustifolia*; Parana pine; Google Earth Engine; UAV-LiDAR; Worldview-2; conservation; Brazil; multi-scale assessment

Citation: Saad, F.; Biswas, S.; Huang, Q.; Corte, A.P.D.; Coraiola, M.; Macey, S.; Carlucci, M.B.; Leimgruber, P. Detectability of the Critically Endangered *Araucaria angustifolia* Tree Using Worldview-2 Images, Google Earth Engine and UAV-LiDAR. *Land* **2021**, *10*, 1316. https://doi.org/10.3390/land10121316

Academic Editors: Wayne Myers and Kristen Brubaker

Received: 23 October 2021
Accepted: 16 November 2021
Published: 30 November 2021

1. Introduction

Global changes resulting from human activities (e.g., urban development, agricultural conversion) are widespread and have been resulting in dramatic declines in global biodiversity [1–4]. Rapid land conversions in biodiversity hotpots are likely to have some of the most significant negative impacts [5–8]. For example, the Brazilian Atlantic Forest (Mata Atlântica) has been reduced substantially, with only 11.4–16.0% of the original extent persisting [6]. A large proportion of the remaining forest fragments (32–40%) are in patches smaller than 100 ha [6,9]. In addition, some of the biologically important tree species, such as the Parana pine (*Araucaria angustifolia*), may be more severely affected by these forest declines than previously thought [6,9].

A. angustifolia is a keystone plant resource in the Brazilian Atlantic Forest because of its importance for increasing structural complexity, phylogenetic diversity and biodiversity

as well as for supporting complex food webs [10–12]. This large and unique conifer species is characterized by a candelabra-shaped crown and is considered highly valuable. Its seeds and wood represent important economic resources for people in southern Brazil [11,13]. However, because of overexploitation, *A. angustifolia* is threatened by extinction. It is classified as endangered (EN) by the Brazilian Red List [14] and critically endangered (CR) by the IUCN Red List [15]. Previous conservation assessments of the Brazilian Atlantic Forest were limited to mapping overall forest cover and decline and to delineating very generalized forest types [6]. No recent and detailed information exists on the remaining distribution and population status of *A. angustifolia*, despite the obvious importance of this tree for maintaining healthy Atlantic Forest ecosystems and for conserving biodiversity [6,13].

Advances in remote sensing technology (unmanned aerial vehicles, UAVs) and geoprocessing analyses (e.g., Google Earth Engine, GEE) provide new and exciting opportunities to accurately delineate, measure and monitor species and habitat types [16–20]. These advances benefit from the increased availability of remote sensing data collected at different altitudes by different platforms (e.g., satellite, airplane, unmanned aerial vehicles) [21–23], the use of new sensors (e.g., LiDAR, hyperspectral) [24–28], improvements in the radiometric and spatial resolution of the data collected [29,30] and vastly enhanced algorithms [22,31–33], including the use of Google Earth Engine to classify diverse types of vegetation [34,35]. The resulting improvements provide technologies for accurately detecting and mapping critical biodiversity conservation targets such as *A. angustifolia*.

In this study, we compare two approaches for detecting, mapping and delineating *A. angustifolia* at different scales—the stand and the individual tree level. Our approach integrates multispectral and object-based classification in a machine learning environment to delineate *A. angustifolia* stands from Worldview-2 images, UAV-based Light Detection and Ranging (LiDAR) and field data to improve validation and to assess our ability to accurately map *A. angustifolia*. Our research questions were as follows:

1. Can *A. angustifolia* canopies be accurately delineated using multispectral classification of pan-sharpened Worldview-2 images in Google Earth Engine?
2. When combined with field estimates of crown sizes, is it possible to extrapolate from canopy cover the number of *A. angustifolia* trees?
3. How different are estimates of numbers of trees based on crown segmentation from UAV-LiDAR imagery and estimates based on multispectral analysis of Worldview-2 images?

2. Methods

2.1. Study Sites

We mapped *A. angustifolia* across three study sites using different remote sensing approaches (Table 1). These sites are spread across different municipalities in the state of Paraná, Brazil (Figure S1), representing variation in the *Araucaria* population, age and spatial distribution. Among these sites, Capão do Tigre has the densest distribution of older *Araucaria* trees while the others have a mixture of young *Araucaria* and other plantations.

Table 1. Study site details and remotely sensed data availability for each site.

Site	Location	Area (ha)	Worldview-2	UAV-LiDAR
Canguiri Farm	Quatro Barras	103.79 ha	Available	Not available
Capão do Tigre	Curitiba	4.45 ha	Available	Available
Gralha-Azul Farm	Fazenda Rio Grande	571.00 ha	Available	Not available

2.2. Data

2.2.1. Worldview-2

Worldview-2, a commercial satellite owned by DigitalGlobe, provides high-resolution, multispectral satellite imagery. It has a panchromatic spatial resolution of 0.46 m ground sample distance (GSD) at nadir and 0.52 m GSD at 20 degrees off-nadir and a multispectral spatial resolution of 1.84 m GSD at nadir, with a revisit time of 1.1 days, and 2.08 m GSD

at 20 degrees off-nadir, with a revisit time of 3.7 days. It has eight multispectral bands: coastal, blue, green, yellow, red, red edge, near-infrared 1 and near-infrared 2. Worldview-2 images are not free, but we acquired them at no cost through a federal contract between the Smithsonian Institute and NASA. We downloaded a single Worldview-2 image with the lowest cloud cover for each site for the year 2018 from (https://earthexplorer.usgs.gov/; accessed on 18 May 2019). All our images had a cloud coverage of less than 15%.

2.2.2. UAV-LiDAR

In August 2019, we acquired LiDAR data at our Capão do Tigre study site using an LTM Pegasus (Optech Incorporated), a full-waveform digitizer system with a maximum frequency of 500 kHz (12 bits). The resulting data represented a point cloud with a density of 4 points/m^2, an altimeter accuracy of 10 cm and a GSD of 18 cm.

2.2.3. Field Data

We were able to access data from a ground survey conducted by the Centro de Excelência em Pesquisas sobre Fixação Carbono na Biomassa—BIOFIX Lab, Federal University of Paraná, for the Capão do Tigre study site. These data consist of GPS coordinates for 335 individuals of *A. angustifolia* [36].

2.3. Methodology

Our overall workflow (Figure 1) included two main approaches:

(a) Map *Araucaria* forest stands across all three study sites using Worldview-2.
(b) Estimate the population of *Araucaria* trees at one study site using UAV-LiDAR.

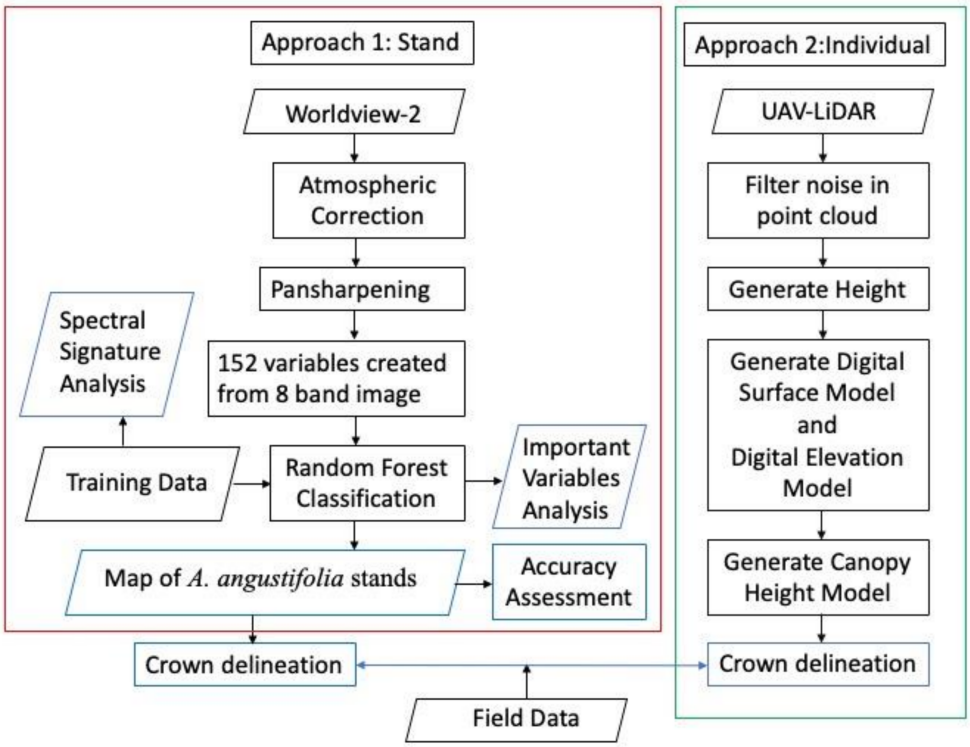

Figure 1. Workflow for mapping *Araucaria angustifolia* stands and individual tree crowns using high-resolution satellite data (i.e., Worldview-2) or UAV-based LiDAR in Brazilian Atlantic Forest, Parana, Brazil.

2.3.1. Mapping Extent of *Araucaria* Forests across All Three Study Sites Using Worldview-2

To reduce the data volume and processing time we clipped the downloaded images to the regions of interest. We performed radiometric correction and applied an atmospheric

correction using the Fast Line-of-sight Atmospheric Analysis of Hypercubes algorithm—FLAASH [37]. To visually enhance the multispectral data, we pan-sharpened [38] the images using ENVI. Pan-sharpening improved the resolution of our pixels from 2 to 0.5 m (see product specifications by DigitalGlobe; https://dg-cms-uploads-production.s3.amazonaws.com/uploads/document/file/98/WorldView2-DS-WV2-rev2.pdf; accessed on 18 May 2019). We then clipped each image again, selecting the forested portions in our study area and excluding cities, roads and buildings using ArcGIS. We used all spectral bands in our analysis.

To classify the Worldview-2 images and differentiate *A. angustifolia* from other species, we used a pixel-based approach with supervised classification. As the data input, we included all spectral bands from our Worldview-2 images as well as a number of remote sensing indices, measures of variation in spectral reflectance and texture indices. Table 2 provides a complete list of the 152 variables entered into our analysis.

Table 2. Variables derived from Worldview-2 spectral bands and entered into supervised classification of *Araucaria* forest.

Abbreviation	Feature [1]
b1	Worldview-2 Coastal Band
b2	Worldview-2 Blue Band
b3	Worldview-2 Green Band
b4	Worldview-2 Yellow Band
b5	Worldview-2 Red Band
b6	Worldview-2 Red Edge Band
b7	Worldview-2 Near Infrared Band 1
b8	Worldview-2 Near Infrared Band 2
asm	Angular Second Moment
contrast	Contrast
corr	Correlation
svar	Sum of Squares: Variance
idm	Inverse Difference Moment
savg	Sum Average
var	Sum Variance
sent	Sum Entropy
ent	Entropy
dvar	Difference Variance
dent	Difference Entropy
imcorr1	Information Measures of Correlation 1
Imcorr2	Information Measures of Correlation 2
maxcorr	Maximal Correlation Coefficient
diss	Dissimilarity
inertia	Inertia
prom	Prominence
shade	Shade

[1] All statistical indices were calculated for all bands. To identify the specific band, each index abbreviation is preceded by the band abbreviation.

For our supervised classification, we relied on the Random Forest (RF) algorithm implemented in Google Earth Engine (GEE). This is a new RF algorithm that was developed for the Statistical Machine Intelligence and Learning Engine (Smile) library (https://haifengl.github.io/; accessed on 18 February 2021) [39], which is now widely used for classifying satellite imagery. This RF algorithm constructs multiple and random decision trees that are bootstrapped to classify a dataset and allows the analyst to control data noise and avoid overfitting [40]. In general, RF algorithms appear to be very robust, allowing for the integration of large sets of variables while reducing the problem of overfitting [40–43]. We digitized a total of 1120 training polygons delineating areas with *A. angustifolia* tree crowns (n = 560) and areas without (i.e., other forests; n = 560). The training polygons were distributed across our three study areas with 120 at Capão do Tigre, 300 at Canguiri Farm

and 700 at Gralha-Azul Farm. We used all pixels contained in the training polygons as input for the supervised classification. This included 2857 training pixels at Capão do Tigre, 11,275 at Gralha-Azul Farm and 1828 at Canguiri Farm. Based on these training data, we ran RF in GEE with 500 random trees (number of trees obtained after generating an ROC curve and an AUC measure) for each study site.

2.3.2. Estimating the Number of *Araucaria* Trees at One Study Site Using UAV-LiDAR

We relied on LAStools (https://rapidlasso.com/lastools/; accessed on 20 June 2020), a widely used open-source tool for processing and filtering LiDAR data [44]. Specifically, we applied LASthin and LASnoise to clean the data and LASground and LASheight to generate the height data needed for detecting *A. angustifolia* crowns. To generate a digital surface model (DSM) and a digital elevation model (DEM) based on the point cloud data, we used ENVI LiDAR software. Finally, we imported the DSM and DEM into R statistical software [45] to create a canopy height model (CHM) for further analysis.

To define the limits of each crown based on the CHM, we relied on the watershed segmentation algorithm [46] provided by the "ForestTools" package in R [47]. The watershed segmentation algorithm requires a function that specifies a dynamic search window for delineating crowns based on canopy height. For our analysis, we used a simple linear equation:

$$f(y) = a \times x + b$$

where x corresponds to the height of the trees and y represents the crown radius. This formula creates a radius within which we can check for similarities in canopy height and use these similarities to delineate crowns. We experimented with different values for a and b to provide the best visual fit for *Araucaria* crowns from the LiDAR data. The final values for our study area were a = 0.2 and b = 0.25.

To automatically separate tree crowns of *A. angustifolia* from other crowns at the Capão do Tigre study site, we first extracted crown characteristics using a zonal summary algorithm (i.e., crown perimeter, area and mean, maximum and standard deviation of LiDAR values within the crown). We utilized the resulting variables in a random forest classification of crowns into *A. angustifolia* and other trees (randomForest package [48]). For training we identified 20 crowns for both *A. angustifolia* and other species [38]. The UAV-LiDAR provided a direct count, i.e., each mapped polygon corresponded to an individual tree.

2.3.3. Analysis

After our classification using RF in GEE, we generated two classes: *A. angustifolia* and other forests. We selected 100 random pixels inside each class boundary and extracted the wavelength values of each pixel using the "raster" package. We assessed the differences in the spectral signatures of *A. angustifolia* and other forests using boxplots in R software [45].

After RF classification in GEE, we extracted the importance of all variables using the ee.Classifier.explain() function. The variables were ranked in descending order of their importance. A visual inspection of the graph of variable importance vs. variable yielded the threshold for determining the most important variables.

We used the classified map of *Araucaria* to determine the extent of *Araucaria* at each study site. The number of pixels classified as *Araucaria* was multiplied by the size of each pixel (0.5 m) to determine the total *Araucaria* extent at each study site.

We used a simple equation that utilizes published data on average crown diameters for *A. angustifolia* trees from Klein (2017) [49] and divided the total area mapped by the average crown size of 10.8 m.

2.3.4. Accuracy Assessment

We evaluated all our products for their accuracy, including the following:

(a) An assessment of how well our pixel-based classification of Worldview-2 images can separate *A. angustifolia* stands from other forests across all three study sites.

(b) The accuracy of estimating the number of *A. angustifolia* trees based on a simple model relating areas of *A. angustifolia* canopy from Worldview-2 to the number of individual trees at the Capão do Tigre study site.
(c) The accuracy of counting all *A. angustifolia* trees using object-based classification of tree crowns using UAV-LiDAR data at the Capão do Tigre study site.

For all the study sites, we evaluated the classification of *A. angustifolia* canopies vs. canopies of other species with Worldview-2. For this, we used out-of-bag (OOB) estimates provided by the RF algorithm in GEE. The OOB estimate uses 30% of the training data as a validation dataset to measure the accuracy of the classification.

We overlaid the GPS data with our *A. angustifolia* map and determined how many points were missing. For all accuracy estimates involving individual trees at the Capão do Tigre study site, we counted crowns that included an *A. angustifolia* GPS location from the field survey as correctly classified and all other *A. angustifolia* crowns as incorrectly classified. Given the large average crown size for *A. angustifolia* [49], we believe that GPS error only had a minor influence on our study.

At the Capão do Tigre study site, we also compared our ability to estimate the number of individual *A. angustifolia* trees based on our pixel-based, multispectral classification of Worldview-2 and our object-based classification of UAV-LiDAR data.

3. Results

3.1. Spectral Response of A. angustifolia Trees

Although there was a general pattern, *A. angustifolia* trees presented a distinctly different spectral response across the three study sites (Figure S2). At our largest site (Gralha-Azul Farm), *A. angustifolia* exhibited a lower reflectance range than other tree species for bands 2 (blue), 3 (green), 5 (red), 6 (red edge) and 7 (NIR-1) (Figure S3A). At our smallest study site (Capão do Tigre), differences in reflectance appeared mainly for bands 3 (green), 4 (yellow), 5 (red), 6 (red edge), 7 (NIR-1) and 8 (NIR-2) (Figure S3B). At Canguiri Farm, reflectance was higher for *A. angustifolia* for bands 3 (green), 4 (yellow), 5 (red), 6 (red edge), 7 (NIR-1) and 8 (NIR-2) (Figure S3C). These differences were also apparent in density plots (Figure S2).

In our pixel-based classification, band b2 (blue) and texture metrics related to variance (dvar, svar and var) were common variables separating *Araucaria* from non-*Araucaria* forests across all of our study sites. Although the most important variables (values above thresholds of 8.96 to 9.92) were different across our study sites, they generally fell into similar categories (Table 3).

Table 3. The most important variables in Random Forest (RF) models for classifying *Araucaria angustifolia* stands from Worldview-2 imagery.

Sites	Threshold Value	Variables [1] and Importance Values	Accuracy (%)
Canguiri Farm	9.98	b5_ent (10.85), b3_dvar (10.17), b2_svar (9.98)	93. 69
Capão do Tigre	8.94	b7_savg (11.30), b6 (9.12), b8 (9.03), b2_var (8.94)	97.14
Gralha-Azul Farm	8.96	b7_shade (10.33), b1_savg (9.37), b6_savg (9.09), b6_dvar (9.05), b2_shade (8.96)	97.63

[1] Variable abbreviations: b1-8 refers to the band number of the original spectral bands provided in Worldview-2 images. The band number is followed by the variable names which are explained in Table 2.

At Capão do Tigre, bands b2 (blue), b6 (red edge), b7 (NIR-1) and b8 (NIR-2) and the texture metrics savg and var helped to separate the *Araucaria* from the non-*Araucaria* forests (Table 3). Previous studies [50,51] have shown that red edge and NIR-1 and -2 bands are helpful in mapping coniferous tree species in the boreal region. The texture metric variance (var) implies the characteristic shape of the *Araucaria* crown, while the sum of

average (savg) is related to the thick *Araucaria* stem volume [52]. These variables reflect the characteristic physical parameters of *Araucaria* and contribute to its separation from surrounding forests with high accuracy (97.14%) (Table 3).

At Gralha-Azul Farm, in addition to the bands (b2, b6 and b7) and texture metrics (savg and dvar) discussed above, band b1 (coastal band) and the texture metric shade were important in separating *Araucaria* from non-*Araucaria* forests with high accuracy (97.63%) (Table 3). Band b1 is mainly used for coastal studies but in vegetation analysis is related to the chlorophyll content of plants [53]. It has been found to be helpful in separating Scots pine, which is similar to *Araucaria* [53]. Cluster shade, which is a measure of the degree of asymmetry, was also helpful in the separation *Araucaria* at this site.

At Canguiri Farm, apart from b2, dvar and svar, the important variables included bands b3 (green) and b5 (red) and entropy (ent). This site contains a number of plantations along with *Araucaria*, so the important variables reflect the separation of different tree species with similar structures, and it has the lowest accuracy (93.69%) among the three sites (Table 3).

3.2. Mapping Araucaria angustifolia Using High-Resolution Satellite Imagery

By using random forest classification of pan-sharpened, high-resolution satellite imagery, we were able to delineate stands of *A. angustifolia*, ranging from individuals to large groups of trees, based on their unique multispectral characteristics (Figure 2). *Araucaria angustifolia* was the dominant canopy tree at Capão do Tigre (56.49% of the canopy; Table 4), less dominant at Canguiri Farm (32.55%; Table 4) and relatively sparse at Gralha-Azul Farm (15.35%; Table 4).

Table 4. Canopy area and percent cover of *Araucaria angustifolia* across three study sites in Paraná, Brazil.

Sites	Total Forest (ha)	*A. angustifolia* (ha)	No. of *A. angustifolia*	*A. angustifolia* Density (Trees/ha)
Canguiri Farm	103.79	33.78 (32.55%)	3668	35.34
Capão do Tigre	4.45	2.52 (56.49%)	280	62.92
Gralha-Azul Farm	571.00	87.65 (15.35%)	9570	16.76

We made a rough estimate of *A. angustifolia* abundance (i.e., number of trees) by dividing the area of *A. angustifolia* stands by the average crown size for the species (Table 4). Based on this calculation, we estimated that there were at least 13,518 trees distributed across our three study areas. The abundance and density of *A. angustifolia* trees were very different across our sites, with higher densities at the smaller sites (Table 4).

3.3. Validation—Random Forest

The accuracy for separating *A. angustifolia* from other species at all study sites was high, with an overall "out-of-bag" accuracy of 0.9369 (93.69%) for Gralha-Azul Farm, 0.9763 (97.63%) for Capão do Tigre and 0.9714 (97.14%) for Canguiri Farm (Table 5).

Based on a ground survey at Capão do Tigre, we found that our Worldview-2 map was nearly 90% accurate in delineating *A. angustifolia* stands (Figure 3A). While the ground survey detected 335 *A. angustifolia* individuals, our crude estimate, derived from dividing the stand area by the average crown size, counted only 280. This value represents an accuracy of 79% in estimating the local *A. angustifolia* population. The omissions (21%) were likely due to the inability to map understory trees of *A. angustifolia* using optical remote sensing data from Worldview-2. In our ground survey data, there are 43 individuals with an average DBH of 18.52 cm, which likely do not reach the canopy.

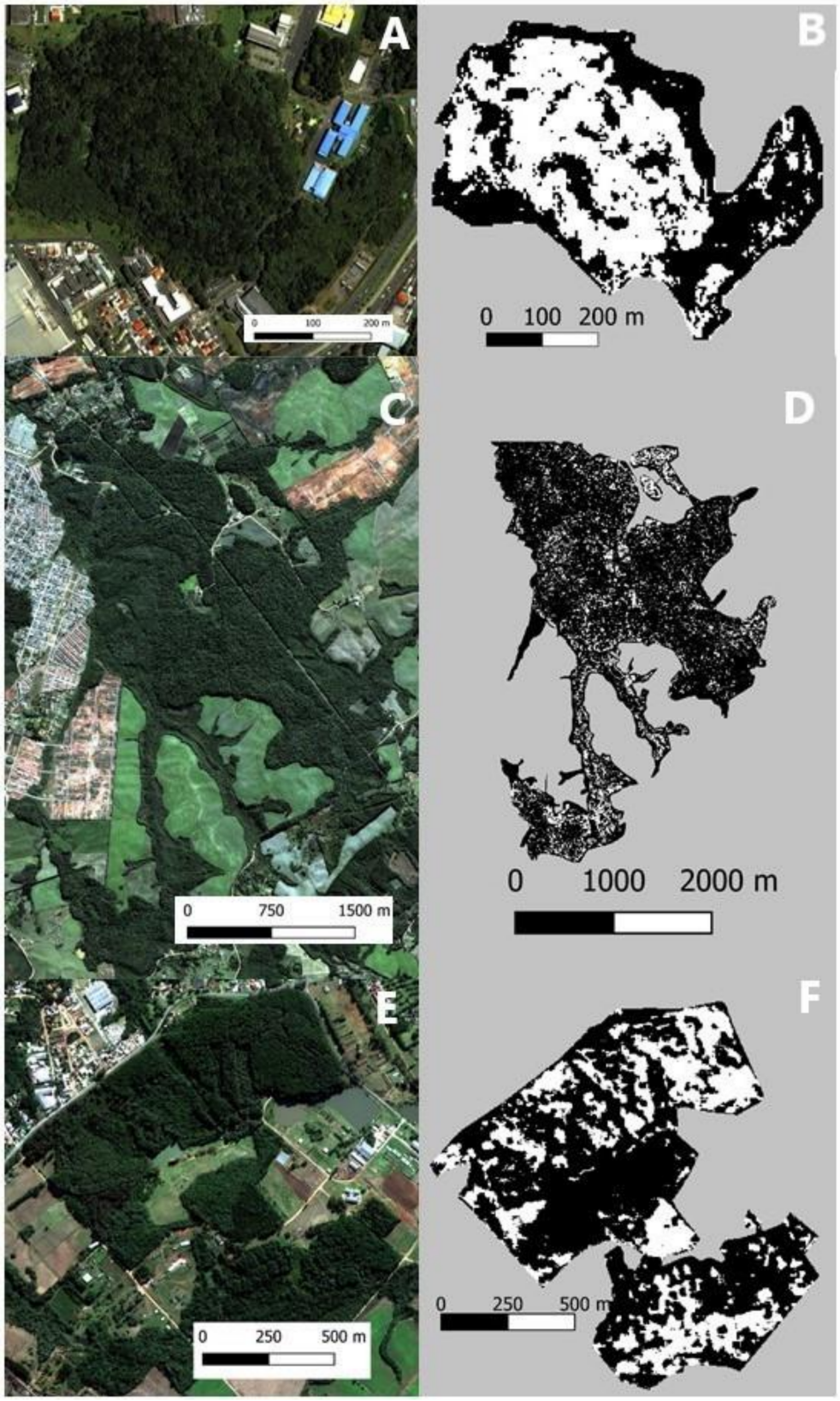

Figure 2. Worldview-2 RGB image (**A**,**C**,**E**) and resulting forest canopy maps delineating *Araucaria angustifolia* stands and trees using a Random Forest classifier (**B**,**D**,**F**) across three study areas in Parana, Brazil. *Araucaria angustifolia* trees are in white; other forest tree species are in black. (**A**,**B**) Capão do Tigre; (**C**,**D**) Gralha-Azul Farm; (**E**,**F**) Canguiri Farm.

Table 5. Commission and omission errors for pixel-based classification of *Araucaria angustifolia* from Worldview-2 images across three study sites in the Brazilian Atlantic Forest of Paraná, Brazil.

			Classified Data			
	Study Area		***Araucaria***	**Non-*Araucaria***	**Total**	**Commission Error (%)**
Reference Data	Gralha-Azul Farm	*Araucaria*	1901	196	2097	9
		Non-*Araucaria*	129	2926	3055	4
		Total	2030	3122	5152	
		Omission error (%)	6	6		
	Canguiri Farm	*Araucaria*	407	11	418	2
		Non-*Araucaria*	12	340	352	3
		Total	419	351	764	
		Omission error (%)	2	3		
	Capão do Tigre	*Araucaria*	979	17	996	1
		Non-*Araucaria*	12	132	144	8
		Total	991	149	1140	
		Omission error (%)	1	11		

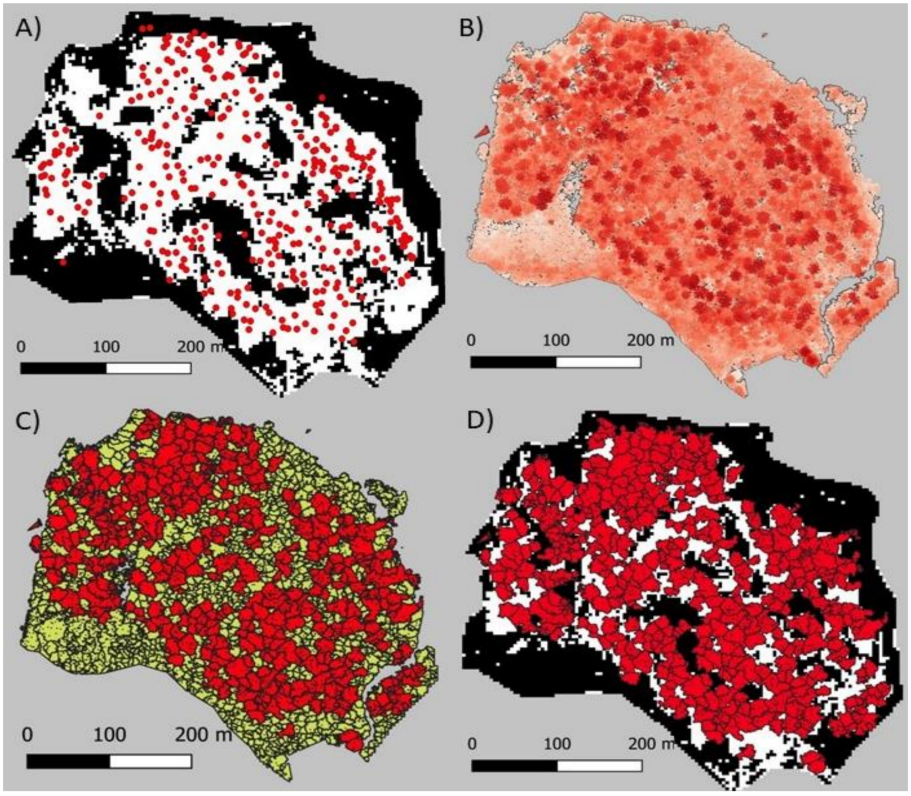

Figure 3. (**A**) Validation for *Araucaria angustifolia* map based on a Random Forest (RF) classification of Worldview-2 imagery at the Capão do Tigre study site in Paraná, Brazil. Red dots are the GPS points of 335 *A. angustifolia* individuals identified on the ground. White = *A. angustifolia* stands from classification, black = other forests. (**B**) Canopy height model (CHM) derived from LiDAR data collected via unmanned aerial vehicle (UAV) for Capão do Tigre; height increases from light to dark red. (**C**) Tree crowns delineated using watershed segmentation; crowns in red are *A. angustifolia* and crowns in green are other species. (**D**) Cross-validation: Red polygons are *A. angustifolia* detected using LiDAR, white raster areas represent *A. angustifolia* areas delineated using RF classification of the Worldview-2 approach and black areas represents other tree species.

3.4. LiDAR Analysis and Validation

Using object-oriented classification of LiDAR data, we were able to account for almost all the *A. angustifolia* individuals found at Capão do Tigre (Figure 3). We detected 351 *A. angustifolia* individuals (Figure 3C). Compared to our ground survey, the algorithm did not find 12 *A. angustifolia* trees (6% omission error) and misidentified 16 crowns of other trees as *A. angustifolia* (31% commission error), with a producer's accuracy of 94% and a user's accuracy of 69% (Table 6). Our validation of the LiDAR and Worldview-2 maps indicates that the tree crowns identified by LiDAR were fully contained in areas classified as *A. angustifolia* with Worldview-2 (Figure 3D). LiDAR provided a higher resolution and identification of individual trees, but Worldview-2 may provide a better representation of the actual canopy cover/overlap with other tree species based on the physical characteristics of the trees, which is the most important factor to classify this species with LiDAR. The percent canopy cover was 84% for *A. angustifolia* and 16% for other canopy tree species. We obtained kappa values of 0.99 for all our study sites.

Table 6. Error matrix for classification of *Araucaria angustifolia* from LiDAR images in Capão do Tigre, Brazilian Atlantic Forest, Parana, Brazil.

		Classified Data			
		Nº of *A. angustifolia*	**Nº of Other Species**	**Total**	**Commission Error (%)**
Reference Data	Nº of *A. angustifolia*	315	142	457	31
	Nº of Other Species	20	954	974	2
	Total	335	1096		
	Omission Error (%)	6	13		

4. Discussion

A. angustifolia is a highly endangered keystone plant resource and is considered the indicator species of the *Araucaria* mixed forest—one of the most important and diverse Atlantic Forest types [10,11]. *Araucaria* mixed forest is rich in biodiversity, especially phylogenetic diversity, because it is composed of lineages from very different moments of the evolutionary history of vascular plants [11] and it forms mosaics with native montane grasslands [12]. Despite their biological significance and importance, *Araucaria* mixed forests are highly threatened following over a century of severe habitat fragmentation, caused mostly by logging and conversion to other land uses [6,13]. Yet, we currently do not have up-to-date information on the species' status and distribution, and techniques for better mapping and monitoring this species have not been made accessible to forest managers and conservation practitioners.

We explored the utility of two remote sensing technologies for detecting and mapping endangered *A. angustifolia* forest stands, delineating individual tree crowns and estimating *A. angustifolia* abundance. Using high-resolution, pan-sharpened Worldview-2 imagery, we were able to delineate *A. araucaria* stands and separate them from other forest types with very high accuracy (i.e., >93%). We were able to do this consistently across multiple sites that varied in percent *A. araucaria* canopy cover between 15% and 57%. We found that *A. angustifolia* canopies had distinct spectral response patters that allowed for separation from other forest types. Variations in spectral response patterns and variable importance between study sites, as observed in our study, are likely due to differences between the study sites in the following:

(a) The density of *A. angustifolia* individuals, where low densities (i.e., small sample sizes in training data) may result in less distinct differences from other forest types;
(b) The age and species composition of interspersed forest types.

Our study demonstrates that powerful machine learning algorithms, such as the RF implemented in the SMILE library used by GEE, are highly successful in detecting *A. angustifolia* and separating this forest type from other forests. This can partly be attributed

to the simple classification system in which we separate only two forest categories (i.e., *Araucaria* vs. other forest) and the fact that accuracy tends to decrease with an increase in classification categories [54,55]. However, most of the success is likely due to the distinct differences in the tree crown and canopy structure as well as the spectral responses of *A. angustifolia* leaves compared to other species [49]. In contrast to broadleaved tees, conifers have lower absorption and higher reflectance in the red band because needle leaves generally have a lower chlorophyll content (i.e., absorb less red light) than broadleaves [56]. Similarly, conifer trees exhibit lower reflectance in the near-infrared bands because conifer leaves usually have a lower water content [57,58]. As is typical for coniferous trees and forests, the blue band helped to separate coniferous *Araucaria* from other deciduous non-*Araucaria* forests. In addition, the characteristically star-shaped texture of *Araucaria* trees was reflected in several measures of variance, such as difference in variance (dvar), sum of squares of variance (svar) and variance (var); these measures were important for delineating *Araucaria* forest across all three sites. These differences are reflected in the very high accuracies across our study sites, ranging from 93.69% to 97.14%.

An alternative explanation for the combination of high accuracies and differences in variable importance may be that our RF models suffered from overfitting [59]. This has been reported for the use of random forest for tropical forest carbon mapping [60]. However, most research on this subject indicates that RF is robust to the inclusion of large numbers of variables [41–43] and can handle high data dimensionality and multicollinearity well [61]. Even Mascaro et al. [60] stated that despite potential issues with overfitting, RF models performed best.

We believe that mapping of *A. angustifolia* forests using supervised classification of spectral data from Worldview-2 imagery is technically feasible. Our results are consistent with previous research, albeit less detailed and more limited, on mapping *A. angustifolia* from high-resolution imagery. Using fuzzy logic and K-nearest neighbor (KNN) applied to Quickbird II images at 3-meter resolution, Pesck et al. (2018) delineated individual *A. angustifolia* crowns at one site in the National Forest of Irati, Paraná [62]. They studied just one site, with homogeneous characteristics. We showed that there might be differences between study sites in terms of reflectance, which can be explained based on the density of *A. angustifolia* in each area. Therefore, studying only one site is not enough to develop a more general algorithm that, in the future, may be able to identify *Araucaria* crowns over broad spatial scales. Mapping at finer scales enabled us to further improve the separation of *A. angustifolia* from other trees with a similar spectral signature.

We also evaluated whether it was possible to develop coarse estimates of *A. angustifolia* abundance and local population size by dividing mapped canopy areas by an average *A. angustifolia* crown size. There are at least two sources of potential error with this method: (a) overlapping crowns may allow for many more *A. angustifolia* trees in one area, and (b) there may be many *A. angustifolia* individuals that are too young to reach the canopy. Both would result in an underestimation. Indeed, when compared to the known number of *A. angustifolia* trees at Capão do Tigre, we missed about 21% of the trees.

UAV-LiDAR, however, proved to be highly accurate in delineating individual *A. angustifolia* crowns, although we likely missed individual trees in the sub-canopy. The use of LiDAR in forest monitoring is still limited, especially in the southern hemisphere. A recent review of 50 LiDAR studies showed a strong bias for research in temperate zones, with only two papers for tropical regions [63]. However, NASA's recent launch of the Global Ecosystems Dynamics Investigation (GEDI) instrument to the International Space Station (ISS) represents a critical new opportunity to expand the use of LiDAR for large-scale biodiversity monitoring [64] and to fill critical knowledge gaps. While GEDI cannot be used to map individual *A. angustifolia* trees, it will be useful to assess whether forest communities with a high abundance of *A. angustifolia* have greater vertical complexity and how this might add to biodiversity in the Brazilian Atlantic Forest.

In our study, we tried to elucidate how UAV-LiDAR may be used to reliably map individual *A. angustifolia* trees. Generally, crown detection and tree mapping can be

challenging even with LiDAR, and many existing studies rely on complex algorithms and extensive code development (e.g., [20]). New advances that integrate high-resolution optical imagery and LiDAR data with deep learning and artificial intelligence algorithms, such as convolutional neural networks (CNNs), have shown tremendous promise for reliably and accurately identifying individual trees (or similar objects) for automated mapping [65,66]. Given the good results using machine learning with Worldview-2 images and LiDAR, we believe that CNNs could be applied successfully in the future to expand on our efforts and for more broad-scale application. In addition, more advanced segmentation algorithms for LiDAR data may also be helpful to detect and delineate individual *A. angustifolia* crowns more reliably.

We compared the two approaches adopted in terms of image/data availability, cost of accessing the data, spatial resolution, scale of detection, detection of *A. angustifolia* and accuracy. In terms of image/data availability, there is a higher chance of finding a Worldview-2 image for a random study site than finding UAV-LiDAR data for the same. Out of our three selected sites, all had a Worldview-2 image with low cloud cover available within the study timeframe, whereas only one site had UAV-LiDAR data available. Wordview-2 images are not free, but similar imagery has been obtained via data purchases by federal agencies in Brazil and the USA. Comparatively, conducting UAV-LiDAR surveys is expensive considering the instrument, sensors, expertise and labor involved. Thus, the cost of images/data is more favorable for Worldview-2. The spatial resolution of UAV-LiDAR data can be adjusted by modifying the flight height depending on the purpose of application, while the spatial resolution of Worldview-2 is fixed. In our case, the resolution of the UAV-LiDAR data was much finer than that of the Worldview-2 images, allowing the detection of individual *A. angustifolia* trees where tree canopies did not overlap, while Worldview-2 images mapped *A. angustifolia* stands with overlapping canopies. Furthermore, UAV-LiDAR provides information on tree height, so neighboring crowns of the same height are considered to belong to the same tree. It cannot differentiate between tree species unless they can be separated by height information. Comparatively, the eight bands of Worldview-2 can separate *A. angustifolia* from other species based on spectral information. In terms of accuracy, UAV-LiDAR was more accurate in the detection of individual *A. angustifolia* trees compared to Worldview-2 due to its finer spatial resolution. Overall, it seems that if mapping individual *A. angustifolia* trees is not the objective, using Worldview-2 is a more practical choice for *A. angustifolia* mapping.

5. Conclusions

Our study should be considered a pilot effort to advance the mapping and monitoring of *A. angustifolia* and other similarly threatened keystone tree species. We showed that high-resolution Worldview-2 imagery can be used in combination with powerful machine learning algorithms to reliably map stands of the critically endangered *A. angustifolia.* These analyses can be implemented using open-source platforms, such as GEE and R, that are readily available to a broad audience of resource managers and conservation practitioners. Using these tools, it might be possible to map *A. angustifolia* stands at a range-wide scale.

It may also be possible to use such maps to roughly estimate remaining *A. angustifolia* populations. However, collection of airborne or UAV-LiDAR data would greatly facilitate population monitoring. We showed that open-source analysis packages such as ForestTools in R can be used to accurately assess *A. angustifolia* numbers for smaller forest areas. We compared both these approaches and conclude that, unless mapping individual *A. angustifolia* trees is the desired objective, using Worldview-2 images for analysis is a practical choice.

Supplementary Materials: The following are available online at https://www.mdpi.com/article/10.3390/land10121316/s1, Figure S1. Study sites in the state of Paraná, Brazil. Canguiri Farm—Quatro Barras/PR (25°23′23.06″ S, 49°7′53.4″) (25°39′29.21″ S, 49°17′17.20″ W); Capão do Tigre—Curitiba/PR (25°26′53.01″ S, 49°14′21.74″ W); Gralha-azul Farm (FEGA)—Fazenda Rio Grande/PR (25°39′29.21″ S, 49°17′17.20″ W).; Figure S2. Density plots of spectral responses of *Araucaria angus-*

tifolia and other forest trees in Brazilian Atlantic Forest from Worldview-2 imagery at three study sites, Parana State, Brazil. Bands: 1—Coastal; 2—Blue; 3—Green; 4—Yellow; 5—Red; 6—Red Edge; 7—Near-Infrared 1; 8—Near-Infrared 2. *A. angustifolia* are represented by red curves and other species by blue; Figure S3. Paired boxplot of spectral responses of *Araucaria angustifolia* and other forest trees in Brazilian Atlantic Forest across three study sites in Paraná State, Brazil. Class 1: *A. angustifolia*, Class 0: Other species. Reflectance values were derived from Worldview-2 imagery (Bands: 1—Coastal; 2—Blue; 3—Green; 4—Yellow; 5—Red; 6—Red Edge; 7—Near-Infrared 1; 8—Near-Infrared 2). (A) Gralha-Azul Farm; (B) Capão do Tigre; (C) Canguiri Farm. The right side of the plot shows the Worldview-2 images with the best band composition for visually separating *A. angustifolia* which appears tree crowns as: (A) Dark green; (B) Dark red; (C) Dark gray/green.

Author Contributions: Conceptualization, F.S., P.L., M.B.C., S.B. and Q.H.; methodology, F.S., P.L., M.B.C., S.B., Q.H., A.P.D.C., M.C. and S.M.; formal analysis, F.S., P.L., M.B.C. and S.B.; writing, review, and editing, F.S., P.L., M.B.C. and S.B.; supervision, M.B.C. and P.L.; project administration M.B.C., P.L. and F.S. All authors have read and agreed to the published version of the manuscript.

Funding: This research was funded by the NASA Land Cover and Land Use Change Program, Grant no. NNX17AI14G; and Coordenação de Aperfeiçoamento de Pessoal de Nível Superior—311 Brasil (CAPES)—Finance Code 001, under a master's scholarship to FS and by Capes/Print, grant #88887.311709/2018-00.

Institutional Review Board Statement: Not applicable.

Data Availability Statement: Not applicable.

Conflicts of Interest: The authors declare no conflict of interest.

References

1. Díaz, S.; Settele, J.; Brondizio, E.S.; Ngo, H.T.; Guèze, M.; Agard, J.; Arneth, A.; Balvanera, P.; Brauman, K.A.; Butchart, S.H.M.; et al. (Eds.) *IPBES Summary for Policymakers of the Global Assessment Report on Biodiversity and Ecosys-Tem Services of the Intergovernmental Science-Policy Platform on Biodiversity and Eco-System Services*; IPBES Secretariat: Bonn, Germany, 2019.
2. Pimm, S.L.; Jenkins, C.N.; Abell, R.; Brooks, T.M.; Gittleman, J.L.; Joppa, L.N.; Raven, P.H.; Roberts, C.M.; Sexton, J.O. The biodiversity of species and their rates of extinction, distribution, and protection. *Science* **2014**, *344*, 1246752. [CrossRef] [PubMed]
3. Pereira, H.M.; Leadley, P.W.; Proença, V.; Alkemade, R.; Scharlemann, J.P.W.; Fernandez-Manjarrés, J.F.; Araújo, M.B.; Balvanera, P.; Biggs, R.; Cheung, W.W.L.; et al. Scenarios for global biodiversity in the 21st century. *Science* **2010**, *330*, 1496–1501. [CrossRef] [PubMed]
4. Myers, N.; Mittermeier, R.A.; Mittermeier, C.G.; Fonseca, G.A.B.; Kent, J. 2013 Potency and Efficacy of a Low Pathogenic H5N2 Inactivated Vaccine Against. *Nature* **2000**, *403*, 853–858. [CrossRef] [PubMed]
5. Brooks, T.M.; Mittermeier, R.A.; Mittermeier, C.G.; Da Fonseca, G.A.B.; Rylands, A.B.; Konstant, W.R.; Flick, P.; Pilgrim, J.; Oldfield, S.; Magin, G.; et al. Habitat Loss and Extinction in the Hotspots of Biodiversity. *Conserv. Biol.* **2002**, *16*, 909–923. [CrossRef]
6. Ribeiro, M.C.; Metzger, J.P.; Martensen, A.C.; Ponzoni, F.J.; Hirota, M.M. The Brazilian Atlantic Forest: How much is left, and how is the remaining forest distributed? Implications for conservation. *Biol. Conserv.* **2009**, *142*, 1141–1153. [CrossRef]
7. Di Marco, M.; Harwood, T.D.; Hoskins, A.J.; Ware, C.; Hill, S.L.L.; Ferrier, S. Projecting impacts of global climate and land-use scenarios on plant biodiversity using compositional-turnover modelling. *Glob. Chang. Biol.* **2019**, *25*, 2763–2778. [CrossRef]
8. Komatsu, K.J.; Avolio, M.L.; Lemoine, N.P.; Isbell, F.; Grman, E.; Houseman, G.R.; Koerner, S.E.; Johnson, D.S.; Wilcox, K.R.; Alatalo, J.M.; et al. Global change effects on plant communities are magnified by time and the number of global change factors imposed. *Proc. Natl. Acad. Sci. USA* **2019**, *116*, 17867–17873. [CrossRef]
9. Zwiener, V.P.; Padial, A.A.; Marques, M.C.M.; Faleiro, F.V.; Loyola, R.; Peterson, A.T. Planning for conservation and restoration under climate and land use change in the Brazilian Atlantic Forest. *Divers. Distrib.* **2017**, *23*, 955–966. [CrossRef]
10. Bogoni, J.A.; Muniz-Tagliari, M.; Peroni, N.; Peres, C.A. Testing the keystone plant resource role of a flagship subtropical tree species (Araucaria angustifolia) in the Brazilian Atlantic Forest. *Ecol. Indic.* **2020**, *118*, 106778. [CrossRef]
11. Duarte, L.D.S.; Bergamin, R.S.; Marcilio-Silva, V.; Seger, G.D.D.S.; Marques, M.C.M. Phylobetadiversity among forest types in the Brazilian Atlantic Forest complex. *PLoS ONE* **2014**, *9*, e0105043. [CrossRef]
12. Behling, H.; Pillar, V.D.P. Late Quaternary vegetation, biodiversity and fire dynamics on the southern Brazilian highland and their implication for conservation and management of modern Araucaria forest and grassland ecosystems. *Philos. Trans. R. Soc. B Biol. Sci.* **2007**, *362*, 243–251. [CrossRef] [PubMed]
13. Koch, Z.; Corrêa, M. *Araucária: A Floresta do Brasil Meridional*; Olhar Brasileiro: Curitiba, Brazil, 2002.
14. Carlucci, M.B.; Prieto, P.V.; Hering, R.L.O.; Judice, D.M.; Monteiro, N.P. Araucariaceae. In *Livro Vermelho da Flora do Brasil*; Martinelli, G., Moraes, M.A., Eds.; Instituto de Pesquisas Jardim Botânico do Rio de Janeiro: Rio de Janeiro, Brazil, 2013; pp. 185–186.

15. Thomas, P. *Araucaria angustifolia*. The IUCN Red List of Threatened Species 2013: e.T32975A2829141. Available online: https://dx.doi.org/10.2305/IUCN.UK.2013-1.RLTS.T32975A2829141.en (accessed on 2 May 2019).
16. Fagan, M.E.; DeFries, R.S.; Sesnie, S.E.; Arroyo-Mora, J.P.; Soto, C.; Singh, A.; Townsend, P.A.; Chazdon, R.L. Mapping species composition of forests and tree plantations in northeastern Costa Rica with an integration of hyperspectral and multitemporal landsat imagery. *Remote Sens.* **2015**, *7*, 5660–5696. [CrossRef]
17. Biswas, S.; Lasko, K.D.; Vadrevu, K.P. Fire Disturbance in Tropical Forests of Myanmar-Analysis Using MODIS Satellite Datasets. *IEEE J. Sel. Top. Appl. Earth Obs. Remote Sens.* **2015**, *8*, 2273–2281. [CrossRef]
18. Batar, A.K.; Watanabe, T.; Kumar, A. Assessment of land-use/land-cover change and forest fragmentation in the Garhwal Himalayan region of India. *Environments* **2017**, *4*, 34. [CrossRef]
19. Woellner, R.; Wagner, T.C. Saving species, time and money: Application of unmanned aerial vehicles (UAVs) for monitoring of an endangered alpine river specialist in a small nature reserve. *Biol. Conserv.* **2019**, *233*, 162–175. [CrossRef]
20. Campbell, M.J.; Dennison, P.E.; Tune, J.W.; Kannenberg, S.A.; Kerr, K.L.; Codding, B.F.; Anderegg, W.R.L. A multi-sensor, multi-scale approach to mapping tree mortality in woodland ecosystems. *Remote Sens. Environ.* **2020**, *245*, 111853. [CrossRef]
21. Getzin, S.; Wiegand, K.; Schöning, I. Assessing biodiversity in forests using very high-resolution images and unmanned aerial vehicles. *Methods Ecol. Evol.* **2012**, *3*, 397–404. [CrossRef]
22. Vadrevu, K.P.; Lasko, K.; Giglio, L.; Schroeder, W.; Biswas, S.; Justice, C. Trends in Vegetation fires in South and Southeast Asian Countries. *Sci. Rep.* **2019**, *9*, 1–13. [CrossRef]
23. Rocchini, D.; Marcantonio, M.; Da Re, D.; Chirici, G.; Galluzzi, M.; Lenoir, J.; Ricotta, C.; Torresani, M.; Ziv, G. Time-lapsing biodiversity: An open source method for measuring diversity changes by remote sensing. *Remote Sens. Environ.* **2019**, *231*, 111192. [CrossRef]
24. Garcia, M.; Ustin, S.L. Detection of interannual vegetation responses to climatic variability using AVIRIS data in a Coastal Savanna in California. *IEEE Trans. Geosci. Remote Sens.* **2001**, *39*, 1480–1490. [CrossRef]
25. Vaglio Laurin, G.; Cheung-Wai Chan, J.; Chen, Q.; Lindsell, J.A.; Coomes, D.A.; Guerriero, L.; Del Frate, F.; Miglietta, F.; Valentini, R. Biodiversity mapping in a tropical West African forest with airborne hyperspectral data. *PLoS ONE* **2014**, *9*, e97910. [CrossRef]
26. Arellano, P.; Tansey, K.; Balzter, H.; Boyd, D.S. Detecting the effects of hydrocarbon pollution in the Amazon forest using hyperspectral satellite images. *Environ. Pollut.* **2015**, *205*, 225–239. [CrossRef] [PubMed]
27. Guo, X.; Coops, N.C.; Tompalski, P.; Nielsen, S.E.; Bater, C.W.; John Stadt, J. Regional mapping of vegetation structure for biodiversity monitoring using airborne lidar data. *Ecol. Inform.* **2017**, *38*, 50–61. [CrossRef]
28. Clark, M.L.; Buck-Diaz, J.; Evens, J. Mapping of forest alliances with simulated multi-seasonal hyperspectral satellite imagery. *Remote Sens. Environ.* **2018**, *210*, 490–507. [CrossRef]
29. Abileah, R. High-resolution imagery applications in the littorals. *Sens. Syst. Next-Gener. Satell. V* **2001**, *4540*, 630. [CrossRef]
30. Waring, R.H.; Coops, N.C.; Ohmann, J.L.; Sarr, D.A. Interpreting Woody Plant Richness from Seasonal Ratios of Photosynthesis. *Ecology* **2002**, *83*, 2964. [CrossRef]
31. Simard, M.; Pinto, N.; Fisher, J.B.; Baccini, A. Mapping forest canopy height globally with spaceborne lidar. *J. Geophys. Res. Biogeosci.* **2011**, *116*, 1–12. [CrossRef]
32. Debastiani, A.B.; Sanquetta, C.R.; Corte, A.P.D.; Rex, F.E.; Pinto, N.S. Evaluating SAR-optical sensor fusion for aboveground biomass estimation in a Brazilian tropical forest. *Ann. For. Res.* **2019**, *62*, 109–122. [CrossRef]
33. Pinto, N.; Keitt, T.H.; Wainright, M. LORACS: JAVA software for modeling landscape connectivity and matrix permeability. *Ecography* **2012**, *35*, 388–392. [CrossRef]
34. Tassi, A.; Gigante, D.; Modica, G.; Di Martino, L.; Vizzari, M. Pixel-vs. Object-based landsat 8 data classification in google earth engine using random forest: The case study of maiella national park. *Remote Sens.* **2021**, *13*, 2299. [CrossRef]
35. Noi Phan, T.; Kuch, V.; Lehnert, L.W. Land cover classification using google earth engine and random forest classifier-the role of image composition. *Remote Sens.* **2020**, *12*, 2411. [CrossRef]
36. Vasconcellos, B.N. Estimativa de Variáveis Dendrométricas Individuais de *Araucaria angustifolia* por Meio de dados Laser Scanner Aéreo e Terrestre; UFPR—Thesis; Universidade Federal do Paraná—Brazil; 1–185. 2020. Available online: https://acervodigital.ufpr.br/bitstream/handle/1884/70292/R%20-%20T%20-%20BRUNA%20NASCIMENTO%20DE%20VASCONCELLOS.pdf?sequence=1&isAllowed=y (accessed on 13 November 2021).
37. *ESRI ArcGIS Desktop: Release 10*; ESRI: Redlands, CA, USA, 2011.
38. Novack, T.; Esch, T.; Kux, H.; Stilla, U. Machine learning comparison between WorldView-2 and QuickBird-2-simulated imagery regarding object-based urban land cover classification. *Remote Sens.* **2011**, *3*, 2263–2282. [CrossRef]
39. Github Statistical Machine Intelligence and Learning Engine (SMILE). Available online: https://haifengl.github.io/classification.html#random-forest (accessed on 18 February 2021).
40. Breiman, L. Random Forests. *Int. J. Adv. Comput. Sci. Appl.* **2016**, *7*, 1–33. [CrossRef]
41. Fox, E.W.; Hill, R.A.; Leibowitz, S.G.; Olsen, A.R.; Thornbrugh, D.J.; Weber, M.H. Assessing the accuracy and stability of variable selection methods for random forest modeling in ecology. *Environ. Monit. Assess.* **2017**, *189*, 316. [CrossRef]
42. Breiman, L. Statistical modeling: The two cultures. *Stat. Sci.* **2001**, *16*, 199–215. [CrossRef]
43. Jagadeesan, S.; Chaturvedi, A.; Kumar, S. URL Phishing Analysis using Random Forest. *Int. J. Pure Appl. Math.* **2018**, *118*, 4159–4163.

44. Montealegre, A.L.; Lamelas, M.T.; De La Riva, J. A Comparison of Open-Source LiDAR Filtering Algorithms in a Mediterranean Forest Environment. *IEEE J. Sel. Top. Appl. Earth Obs. Remote Sens.* **2015**, *8*, 4072–4085. [CrossRef]
45. R Core Team. R: A Language and Environment for Statistical Computing. R Foundation for Statistical Computing: Vienna, Austria. Available online: https://www.R-project.org/ (accessed on 18 November 2021).
46. Meyer, F.; Beucher, S. Morphological segmentation. *J. Vis. Commun. Image Represent.* **1990**, *1*, 21–46. [CrossRef]
47. Plowright, A. Canopy Analysis in R Using Forest Tools. Available online: https://cran.r-project.org/web/packages/ForestTools/vignettes/treetop_analysis.html (accessed on 18 November 2021).
48. Liaw, A.; Wiener, M. Classification and Regression by randomForest. *R News* **2002**, *2*, 18–22.
49. Klein, D.R. *Morfometria e Crescimento Diamétrico de Araucaria Angustifolia (bertol.) Kuntze no Planalto Sul Catarinense*; UFPR: Curitiba, PR, Brazil, 2017.
50. Yang, X.; Rochdi, N.; Zhang, J.; Banting, J.; Rolfson, D.; King, C.; Staenz, K.; Patterson, S.; Purdy, B. Mapping tree species in a boreal forest area using RapidEye and LiDAR data. In Proceedings of the 2014 IEEE Geoscience and Remote Sensing Symposium, Quebec City, QC, Canada, 13–18 July 2014; Volume 14, pp. 69–71. [CrossRef]
51. Adamczyk, J.; Osberger, A. Red-edge vegetation indices for detecting and assessing disturbances in Norway spruce dominated mountain forests. *Int. J. Appl. Earth Obs. Geoinf.* **2015**, *37*, 90–99. [CrossRef]
52. Niemi, M.T.; Vauhkonen, J. Extracting canopy surface texture from airborne laser scanning data for the supervised and unsupervised prediction of area-based forest characteristics. *Remote Sens.* **2016**, *8*, 582. [CrossRef]
53. Immitzer, M.; Atzberger, C.; Koukal, T. Tree species classification with Random forest using very high spatial resolution 8-band worldView-2 satellite data. *Remote Sens.* **2012**, *4*, 2661–2693. [CrossRef]
54. Van Thinh, T.; Duong, P.C.; Nasahara, K.N.; Tadono, T. How does land use/land cover map's accuracy depend on number of classification classes? *Sci. Online Lett. Atmos.* **2019**, *15*, 28–31. [CrossRef]
55. Gessner, U.; Machwitz, M.; Esch, T.; Tillack, A.; Naeimi, V.; Kuenzer, C.; Dech, S. Multi-sensor mapping of West African land cover using MODIS, ASAR and TanDEM-X/TerraSAR-X data. *Remote Sens. Environ.* **2015**, *164*, 282–297. [CrossRef]
56. Croft, H.; Chen, J.M.; Zhang, Y.; Simic, A. Modelling leaf chlorophyll content in broadleaf and needle leaf canopies from ground, CASI, Landsat TM 5 and MERIS reflectance data. *Remote Sens. Environ.* **2013**, *133*, 128–140. [CrossRef]
57. Hall, F.G.; Huemmrich, K.F.; Strebel, D.E.; Goetz, S.J.; Nickeson, J.E.; Woods, K.E. Biophysical, morphological, canopy optical property, and productivity data from the superior national forest. In *NASA Technical Memorandum 104568*; NASA: Greenbelt, MD, USA, 1992.
58. Roberts, D.A.; Ustin, S.L.; Ogunjemiyo, S.; Greenberg, J.; Bobrowski, S.Z.; Chen, J.; Hinckley, T.M. Spectral and structural measures of northwest forest vegetation at leaf to landscape scales. *Ecosystems* **2004**, *7*, 545–562. [CrossRef]
59. Franklin, J. *The Elements of Statistical Learning: Data Mining, Inference, and Prediction*; Springer: New York, NY, USA, 2009.
60. Mascaro, J.; Asner, G.P.; Knapp, D.E.; Kennedy-Bowdoin, T.; Martin, R.E.; Anderson, C.; Higgins, M.; Chadwick, K.D. A tale of two "Forests": Random Forest machine learning aids tropical Forest carbon mapping. *PLoS ONE* **2014**, *9*, 12–16. [CrossRef]
61. Belgiu, M.; Drăgu, L. Random forest in remote sensing: A review of applications and future directions. *ISPRS J. Photogramm. Remote Sens.* **2016**, *114*, 24–31. [CrossRef]
62. Pesck, V.A.; Stepka, T.F.; dos Santos Lisboa, G.; de Jesus França, L.C.; Cerqueira, C.L. Delineamento de copas de *Araucaria angustifolia* utilizando lógica Fuzzy em imagens Quickbird II. *Adv. For. Sci.* **2018**, *5*, 385–390.
63. Bakx, T.R.M.; Koma, Z.; Seijmonsbergen, A.C.; Kissling, W.D. Use and categorization of light detection and ranging vegetation metrics in avian diversity and species distribution research. *Divers. Distrib.* **2019**, *25*, 1045–1059. [CrossRef]
64. Dubayah, R.; Blair, J.B.; Goetz, S.; Fatoyinbo, L.; Hansen, M.; Healey, S.; Hofton, M.; Hurtt, G.; Kellner, J.; Luthcke, S.; et al. The Global Ecosystem Dynamics Investigation: High-resolution laser ranging of the Earth's forests and topography. *Sci. Remote Sens.* **2020**, *1*, 100002. [CrossRef]
65. Guirado, E.; Tabik, S.; Alcaraz-Segura, D.; Cabello, J.; Herrera, F. Deep-learning Versus OBIA for scattered shrub detection with Google Earth Imagery: Ziziphus lotus as case study. *Remote Sens.* **2017**, *9*, 1220. [CrossRef]
66. Weinstein, B.G.; Marconi, S.; Bohlman, S.; Zare, A.; White, E. Individual tree-crown detection in rgb imagery using semi-supervised deep learning neural networks. *Remote Sens.* **2019**, *11*, 1309. [CrossRef]